Soft Matter

PAPER

Surface rheology: macro- and microrheology of poly(*tert*-butyl acrylate) monolayers

Armando Maestro,†[a] Laura J. Bonales,[a] Hernan Ritacco,[a] Thomas M. Fischer,[b] Ramón G. Rubio*[a] and Francisco Ortega*[a]

We have studied the surface shear viscoelasticity of poly(*tert*-butyl-acrylate) Langmuir monolayers spread at the air/water interface, by tracking the Brownian motion of tracer particles with different sizes and surface chemical nature, trapped at the same interface. Surface shear moduli have been extracted from the particles mean square displacements (MSD), using different approaches: hydrodynamic calculations of drag coefficients and direct inversion of the MSD by means of the generalized Stokes–Einstein equation. It has been found that these different theoretical approaches lead to comparable values of the shear interfacial viscosity independent of the polymer concentration and molecular weight. In addition, no effect of the size or chemical nature of the probe has been detected. The results have demonstrated the consistency of the microrheological techniques used, and confirm the existence of entanglements in PtBA monolayers, as recently deduced from dilational elasticity and viscosity measurements, [Maestro *et al.*, *Soft Matter*, 2010, **6**, 4407]. An unexpected result was that the interfacial viscosity values obtained from microrheology have been found to be several orders of magnitude lower than the ones obtained with macroscopic interfacial shear rheometers. At the moment there is no clear explanation for this disagreement, although it is not related to the probe size or their chemical nature. Furthermore, this discrepancy is not related to the analysis methodology used, including the calculation of the two-point correlation function used in 3D microrheology when there are heterogeneities present within the range of the probe size.

1. Introduction

Reducing the dimensions of a polymer film to the nm range modifies some of its equilibrium and dynamic properties.[1,2] Interfaces play a dominant role in the behavior of many complex fluids and interfacial rheology has been found to be a key factor in the stability of foams and emulsions, compatibilization of polymer blends, flotation technology, fusion of vesicles, *etc.*[3–5] Langmuir monolayers at the air/water surface are good systems for studying polymer systems in quasi-two dimensions, and have been extensively described leading to a set of theories and models within the framework of *quasi*-bidimensional polymer solutions.[6,7] It has been found that the surface pressure, Π, and the equilibrium elasticity, ε_0, of polymer monolayers follow power laws of the surface concentration, Γ, with exponents that depend on the so-called solvent-quality of the interface for a given

polymer and temperature.[8,9] The availability of experimental techniques for measuring the interfacial dilational and shear rheology over a broad frequency range, ω, has allowed to measure the complex viscoelastic moduli pointing out that the interfacial elasticity and viscosity can also be described by power laws of ω and of Γ.[10–12] Moreover, the exponents of these laws depend on the solvent-quality of the interface,[13] and coincide with those of the equilibrium properties.[14] However, there has been some discussion about the dynamical mechanism of polymer chains confined to a quasi-two dimensional space, as in a monolayer.[15–21] In a recent work Maestro *et al.*[22] have carried out a detailed study of the M_w-dependence of the equilibrium and rheological properties (dilational and shear interfacial rheology) of monolayers of monodisperse poly(*tert*-butyl acrylate), PtBA, samples over a broad molecular weight range (4–850 kDa) and frequency. Their results confirm the validity of the reptation mechanism to explain the dynamics of polymer monolayers under good solvent conditions.

Krägel *et al.*,[23] Erni *et al.*,[24] Reynaert *et al.*[25] and Barentin *et al.*[26] have described macroscopic rheometers for measuring interfacial shear viscosities. In all these devices the length-scale of the rheometer probe is orders of magnitude bigger than the typical mesh-size of a polymer monolayer[27] in the semidilute

[a]*Departamento de Química Física I, Facultad de Química, Universidad Complutense, 28040 Madrid, Spain. E-mail: fortega@quim.ucm.es; rgrubio@quim.ucm.es*
[b]*Institute of Experimental Physics, The University of Bayreuth, 95440 Bayreuth, Germany*
† Current address: Laboratoire de Physique des Solides, Bâtiment 510, Université Paris-Sud XI, 91405 Orsay, France.

regime and they are limited to low-frequencies (typically below 0.5 Hz). Microrheology is an appropriate technique to explore the shear rheology of monolayers confined to fluid interfaces because the strain imposed on the system is small (therefore the system remains in the linear regime), and it is possible to carry out the study over a broader frequency range.[28,29]

2. Microrheology

Microrheology is a term that does not describe a particular technique, but rather a number of approaches that attempt to overcome some limitations of traditional bulk rheology.[30–33] Advantages over macrorheology include a significantly higher range of frequencies available without time–temperature super-position,[34–36] the capability of measuring material inhomogeneities that are inaccessible to macrorheological methods, and rapid thermal and chemical homogenization that allows the transient rheology of evolving systems to be studied.[36] Microrheology methods typically use embedded micron-sized probes to locally deform the sample, permitting the use of very small volumes (∼μL).

In the case of surface shear rheology, most of the information available has been obtained using macroscopic interfacial rheometers which have a sensibility limit of about 10^{-6} mN s m^{-1},[37–40] but many important systems have surface shear viscosities below this limit. Particle tracking techniques have been foreseen as a powerful method to study the dynamics of interfaces for shear viscosities as low as 10^{-10} mN s m^{-1}.[41,42] However, the first results obtained by this technique show that the shear viscosities obtained are systematically lower than those measured by means of conventional macroscopic rheology on the same systems and conditions (concentration, temperature, etc.).[41,43,44]

Although recent available techniques make the experimental realization of surface microreology relatively straightforward, one has to rely on hydrodynamic models of the monolayer in order to obtain variables such as interfacial elasticity or shear viscosity. The more complex the structure of the interface the stronger are the assumptions of the models thus resulting in more difficulties in checking their validity. In the present work we will present a systematic study of the shear viscosity of monolayers of PtBA formed onto water surfaces by a particle tracking technique. We explore the influence of the chemical nature of the probes on the measured viscosities, the validity of the different theoretical approaches used for analysing the results and we compare the particle tracking results on PtBA with those obtained with conventional surface shear macro-rheometers. We will show the influence that surface concentration and polymer molecular weight have on the monolayer features.

3. Experimental

3.1. Materials

We have used highly monodisperse samples of poly(ter-butyl-acrylate) (PtBA) purchased from Polymer Source (Canada), with molecular weights ranging from 1.44×10^3 to 1.095×10^6 g mol^{-1}. The properties of the samples used are summarized in Table 1. Chloroform (Sigma Aldrich, 99% purity) was used as spreading solvent. The concentration of the spreading solution

Table 1 Properties of poly(ter-butyl-acrylate) used in this study

Commercial name	$M_w/10^{-3}$ g mol^{-1}	$M_n/10^{-3}$ g mol^{-1}	M_w/M_n
P1828-tBA	1.56	1.45	0.93
P2213-tBA	3.47	3.03	0.87
P2532-tBA	4.6	4.0	0.87
P1670-tBA	7.5	7.0	0.93
P1036-tBA	16.3	14.4	0.88
P2009-tBA	21.2	19.6	0.92
P1148-tBA	39.2	37.0	0.94
P1598-tBA	52.1	46.5	0.89
P2450-tBA	103.0	79.0	0.77
P1592-tBA	327.0	287.0	0.88
P346-tBA	1094.8	870.0	0.79

was 0.1 mg ml^{-1} for all the samples. Water from a MilliQ-RG system (resistivity of 18.2 MΩ) was used to prepare the subphase. The protocol for the preparation of the monolayers was the same as described in a previous work[45] and all the experiments have been performed at a fixed temperature of 25.0 °C.

For particle tracking experiments we have used spherical micro-particles of different chemical natures: (a) negatively charged polystyrene (PS) microparticles with sulfate functional groups on the surface (Interfacial Dynamics Corporation, USA) with diameters 1.6 and 5.7 μm and both with a similar surface charge density (≈6 μC.cm^{-2}); (b) poly(methyl methacrylate) (PMMA) microparticles (Microparticles GmbH, Germany) with diameters 1 and 2 μm. The 1 μm-particles are electrostatically stabilized by sulfate groups attached on the particle surface, and the 2 μm-particles are stabilized sterically by grafted chains of poly(vinylacetate), PVAc, physically adsorbed onto their surface; (c) spherical particles of silica (SiO$_2$) of diameter 1 μm containing silanol groups on their surface (Sigma-Aldrich, Germany).

3.2. Techniques and data analysis

3.2.1. Π–Γ Isotherms. The surface pressure, Π, vs. surface concentration, Γ, isotherms of polymer monolayers were measured on a home-made measuring cell that includes a Langmuir trough and that can be placed in the microscope for particle tracking measurements. A paper Wilhelmy plate placed at the air–water interface was used as surface force sensor. Near the interface, the temperature was measured with a precision of 0.01 °C using a PT100 sensor; the temperature stability was better than ±0.05 °C. Care was taken to avoid any changes on the height of the monolayer during the experiments due to evaporation; to this end a leveling system has been included in the measuring cell that allows us to adjust the interface height at the microscope focus. Each Π-value was determined with a precision of ±0.05 mN m^{-1}, and each value reported was the average of five measurements that agreed within the experimental uncertainty. The ratio of the trough to the Wilhelmy plate widths was higher than eight so any influence of the flow field could be neglected.

3.2.2. Contact angles. We have used the gel trapping technique (GTT) to measure the three-phase contact angle of the probe particles trapped at the interface.[45,46] The GTT method has been recently criticized by Horozov et al.[47] on the basis of possible complexation between the polymeric gelling agent

(gellant) and the particles, in our case this is not likely because both are negatively charged. Moreover, gellant was found not to adsorb at the water surface (same surface tension as water and zero surface elasticity). The values of the contact angles obtained with the GTT technique were verified by two other methods: (1) Clint and Taylor's method in which the collapse pressure in the surface pressure–area isotherm is used to determine the contact angle assuming a hexagonal packing of the particle at the collapse;[48] and (2) the excluded area formalism[49] in which a mixed particle-insoluble polymer monolayer is formed and the contact angle is obtained from the slope of the excluded area as a function of surface pressure. This method is valid as far as there are no interactions between particles and the polymer in the monolayer. As we have shown in a previous work,[45] this condition is fulfilled in our case.

One important point that should be stressed here is that the contact angle depends on the solvent used to spread the particles,[45] and the contact angle is a key variable for the hydrodynamic calculations used to estimate the surface shear viscosity from the diffusion coefficient,[43,44,50,51] therefore one has to be very careful when comparing results obtained using different spreading solvents for a given probe particle.

3.2.3. Particle tracking

3.2.3.1. Experimental setup. The setup is based on a Nikon Eclipse 80i microscope with a digital head (variable magnification 0.8× to 2×) and with several long working distance objectives of 10×, 50× and 100× magnification. A CCD high-speed camera (Hamamatsu, model C8800-21C) capable of taking 30 fps at full resolution (1000 × 1000 pixel) was used to record the image sequences. The sequences were transferred to a computer to be analyzed and to extract the 2D trajectories of a set of particles using home-made software.[44] In typical experimental conditions we get 80 nm per pixel and an error in the particle center location of 1/10 pixel, this means that the displacement uncertainty is around 8 nm and the smallest measurable MSD 0.016 μm^2. The average number of particles within the view field was ∼10 in order to prevent particle–particle interactions, and in all the cases it was checked that the radial distribution function of the probe particles did not show any structure.[52]

3.2.3.2. Monoloyers preparation protocols. The mixed Langmuir monolayers formed by polymers and particles were built in two different ways: sequential spreading, and simultaneous spreading of both components on the air–water (A/W) interface. The sequential method consisted in spreading the particles onto the A/W interface when a very dilute polymer monolayer has already been formed and stabilized. When the spreading solvent of the particles was evaporated a mixed layer is created on the A/W interface. It is very important to wait for more than two hours after adding the particles to allow the polymer network to relax from any conformational change induced by the solvent used to spread the particles. In the case of simultaneous spreading, the Langmuir trough of the cell was separated in two well defined sections by a removable barrier, one for the very diluted polymer monolayer and the other one for the particles monolayer. When the spreading solvents have evaporated and the respective monolayers have been formed, the two separated regions are put in contact by removing the barrier. A mixed Langmuir monolayer is created *via* interdiffusion of the polymer and particles. Both methods have led to quantitatively comparable results.

To minimize the macroscopic drift of the particles at the air–water interface due to thermal convection promoted by temperature gradients and air currents along the monolayer, a set of homemade stainless steel rings has been used following previous works of Klinger and McConell,[53] and of Bonales *et al.*[44,52]

3.2.4. Macroscopic shear rheology.
The complex surface shear modulus $G^*(\omega)$ is defined as $G^*(\omega) = G'(\omega) + iG''(\omega) = G'(\omega) + i\omega\eta_s$, where ω is the frequency, and η_s is the surface shear viscosity. Two different experimental devices were used to measure G' and G'' of PtBA monolayers at the air–water interface. The first one was the Interfacial Shear Rheometer ISR-1, from Sinterface (Germany), consisting of a ring with a sharp edge hanging on a wolfram torsion wire. The second rheometer was an Interfacial Shear Rheometer (model MCR301–IRS) from Anton Paar (Austria) that consists of a biconical disk rigidly coupled to a driving motor and to a torque and normal force transducer unit. The edge of the disk is placed in the interface between the two different fluids, air/liquid or liquid/liquid. Further details about the interfacial shear rheology have been described elsewhere.[23,24,54,55] All the experiments were carried out for 1–2% strain, a value well within the linear response range of our monolayers.

4. Data analysis

4.1. Mean squared displacement (MSD)

The main idea in particle tracking is to follow the trajectories (Brownian motion) of the probe particles trapped at the surface by videomicroscopy. The time evolution of the mean square displacement $\langle\Delta r^2(t)\rangle$ of the particles can then be obtained and reflects the response of the material to the stress applied to it by the thermal motion of the probes (passive microrheology). The MSD can be calculated from single particle trajectories or from two particle relative displacements, according to the following equations, where $\Delta\vec{r}$ is a 2D displacement

$$\langle\Delta r^2(t)\rangle_A = \langle\vec{r}(t_0 + t) - \vec{r}(t_0)\rangle = 4Dt^\alpha \quad (1)$$

$$\langle\Delta r^2(t)\rangle_R = \langle[\vec{r}_i(t_0 + t) - \vec{r}_j(t_0 + t)] - [\vec{r}_i(t_0) - \vec{r}_j(t_0)]\rangle = 8Dt^\alpha \quad (2)$$

The subindices A and R refer to the absolute or single particle and relative or two particle MSD. In eqn (1) and (2) the average is collective over all the particles (or pair of particles) in the field of view and also over all the initial times, t_0. For a purely viscous interface and low probe particle density α is equal to 1 and the usual Einstein's linear relation is obtained between the MSD and the lag time, t. Although the experiments have been performed trying to minimize drift movements (see the Experimental section) there is always a residual unavoidable drift which should be eliminated from the experimental MSD's. One of the methods to remove the drift methods is the calculation of the two-particle relative MSD (eqn (2)), alternatively the single particle MSD can

be corrected by subtracting the mean particle displacement averaged over all particles and frames of the sequence, that is to calculate the variance expressed as

$$\langle \Delta r^2(t) \rangle_{\text{VAR}} = \langle \Delta r^2(t) \rangle_{\text{A}} - \langle \Delta \vec{r}(t) \rangle^2 \qquad (3)$$

The last method is analogous to the one used by Corrigan and Donald[56]

The infinite dilution diffusion coefficient, D, that characterizes the Brownian motion of a sphere of radius, a, immersed in a fluid of shear viscosity, η, is related to the friction coefficient, f, by the Einstein relation

$$D = \frac{k_B T}{f} \qquad (4)$$

For three-dimensional systems and a stick boundary flow, f is given by Stokes law, $f = 6\pi\eta a$. In 2D, even for an inviscid interface, f takes a more complex form, being a function of the particle's contact angle and radius, θ and a, respectively, and of the viscosities of the adjacent phases, η_1 and η_2.[50,52] It should be emphasized that in 2D the infinite dilution condition for the diffusion coefficient becomes even more restrictive than in 3D due to the fact that, while in 3D the velocity field decay with particle separation as $\sim r^{-1}$, in strictly 2D becomes long ranged $\sim \log r$. Nevertheless, in quasi-2D conditions, which correspond with the usual experimental conditions, there is a coupling with the bulk fluids adjacent to the interface, and as a consequence a long ranged velocity field is only expected when $\eta_s \gg \eta a$, where η_s is the surface shear viscosity, η the subphase viscosity and a the probe radius. For viscous interfaces there are several methods that allow calculation of the surface shear viscosity from the MSD data of probe particles trapped at those interfaces.

4.2.   Contact angle dependent friction factor calculations

Fischer et al.[50] have numerically solved the fluid hydrodynamics equations for a probe sphere of radius a moving in an *incompressible* interface of surface shear viscosity, η_s between two infinite viscous phases (η_1, η_2), as a function of the contact angle θ of the particle at the interface. The monolayer surface was assumed to be flat (no electrodipping effects) and the translational drag coefficient, f, was expressed as a series expansion in the Boussinesq number, $B = \eta_s/((\eta_1 + \eta_2)a)$:

$$f = \eta_1 a(k_T^0 + Bk_T^1 + O(B^2)) \qquad (5)$$

For the inviscid interface ($B = 0$), and in the case of the air–water interface ($\eta_1 = \eta_w$, $\eta_2 \approx 0$), the numerical results for k_T^0 and k_T^1 are fitted with an accuracy of 3% by the formulae,

$$k_T^0 \approx 6\pi\sqrt{\tanh\left(32\left(\frac{d}{a}+2\right)\Big/(9\pi^2)\right)} \qquad (6)$$

$$k_T^1 \approx -4\ln\left(\frac{2}{\pi}\arctan\left(\frac{2}{3}\right)\right)\left(\frac{a^{2/3}}{(d+3a)^{3/2}}\right)(d/a) > 0$$

$$k_T^1 \approx -4\ln\left(\frac{2}{\pi}\arctan\left(\frac{2}{3}\right)\right)\left(\frac{a^{2/3}}{(d+3a)}\right)(d/a) < 0 \qquad (7)$$

where d is the distance from the apex of the bead to the plane of the interface ($d/a = \cos\theta - 1$). An argument given by Fischer et al.[50] and by Sickert et al.[43] for considering the monolayers as incompressible is that the diffusion of the monolayer material is much faster than that of the probes. Danov et al. made a similar calculation assuming a *compressible* interface,[51] unfortunately their final calculations are only plotted for some specific condition (equal numerical values of the shear and dilational viscosities) which makes them more difficult to apply to interfaces for which the ratio of dilational to shear viscosities is not known "*a priori*". It has been shown that for fatty acid monolayers Fischer's and Danov's theories coincide.[43]

We found that in order for Fischer's[50] or Danov's[51] friction factors calculations to quantitatively describe our experimental friction coefficients of microparticles at bare air/water and oil/water interfaces, it was necessary to multiply the theoretical predictions by an *ad hoc* numerical factor, independent of θ but different for air/water and oil/water interfaces.[42] In the present work we have used the scaled version of Fischer's friction factor calculations for which the diffusion coefficient for microparticles at the air/water interface takes the following form

$$D = \frac{k_B T}{\mathscr{R}\eta_w a\left[k_T^0(\theta) + Bk_T^1(\theta)\right]} \qquad (8)$$

where $\mathscr{R}$ is the scaling factor that for the air/water interface adopts a value of 1.8 ± 0.2. Eqn (8) gives for a microparticle of $a = 0.8$ μm trapped at the bare ($B = 0$) air/water interface with a contact angle of $\theta = 90°$ and at 25 °C a value of $D = 0.2$ μm² s⁻¹ (see Table 2 for comparison). In the present particle tracking experiments B changes from 0.1 for the lower molecular weight PtBA monolayers up to 100 for the highest one. In principle, we may expect eqn (8) to breakdown for the higher molecular weight monolayers as a consequence of the higher order terms in B. Surprisingly, as it will be evident later, eqn (8) gives surface viscosity values in agreement with other theoretical approaches that do not have this limitation.

4.3.   Generalized Stokes–Einstein equation (GSE)

A generalization of the *Stokes–Einstein equation* (GSE) was proposed in 3D which accounts for the full frequency dependence of the shear viscoelastic moduli obtained from the experimental MSD's. Several schemes have been devised for calculating the shear elastic and loss moduli, the simplest Mason's formula is given by:[35]

$$\begin{aligned} G'(\omega) &= |G^*(\omega)|\cos\left[\pi\alpha(\omega)/2\right] \\ G''(\omega) &= |G^*(\omega)|\sin\left[\pi\alpha(\omega)/2\right] \end{aligned} \qquad (9)$$

where the shear modulus, $|G^*(\omega)|$ and the local first-order logarithmic derivative of $\langle \Delta r^2(t) \rangle$, $\alpha(t)$, are given by

$$|G^*(\omega)| = \frac{k_B T}{\pi a\langle \Delta r^2(1/\omega) \rangle \Gamma_E[1 + \alpha(\omega)]} \qquad (10)$$

$$\alpha(t) = \frac{\partial\ln\langle \Delta r^2(t) \rangle}{\partial\ln t} \qquad (11)$$

where Γ_E denotes Euler's Gamma function and $\alpha(\omega)$ is easily calculated from $\alpha(t)$. In eqn (10)) $|G^*(\omega)|$ has 3D units, and

Table 2 Properties of the particles used as probes: diameter (σ), three-phase contact angle (θ) (using methanol as spreading solvent)[45] and the infinite dilution diffusion coefficient measured at a clean air/water interface, D_0

Chemical nature	Diameters, $\sigma/\mu m$	Contact angle $\theta/°$	Diffusion coefficient $D_0/\mu m^2\ s^{-1}$
PS	1.6	89 ± 8	0.216 ± 0.004
	5.7	37 ± 2	0.070 ± 0.020
PMMA	1.0	18 ± 6	0.278 ± 0.002
	2.0	29 ± 4	0.493 ± 0.009
SiO_2	1.0	41 ± 9	0.41 ± 0.05

in order to convert that modulus to 2D ones, it is necessary to introduce a characteristic length of the system that multiplies eqn (10). For macroscopic surface shear rheometers[23–26] and for model membranes[57] the characteristic length is related to the probe dimensions that cause the flow, thus we have used the particle radius, which leads to a 2D analogue of eqn (10))

$$|G^*(\omega)| = \frac{k_B T}{\pi \langle \Delta r^2 (1/\omega) \rangle \Gamma_E [1 + k(\omega)]} \tag{12}$$

An important advantage of the GSE method is that it is possible to obtain G' and G'' from the MSD data, provided that the local power-law assumption $\langle \Delta r^2(t) \rangle \approx t^\alpha$ is fulfilled, with α between 0 and 1 corresponding to a purely elastic or viscous material, respectively. This approach has been recently applied to quasi-2D systems[58] and at present is the only method that allows to apply passive microrheology to viscoelastic interfaces, in contrast to hydrodynamic calculations that strictly apply to purely viscous interfaces. In the previous reference J. Wu et al. report "apparent" surface modulus with 3D units, using eqn (10)). When comparing this GSE approach with the previous hydrodynamic treatments it must be considered that with GSE we will find a shear storage modulus that will entirely be due to the monolayer, and a loss one that will have two components: a frequency independent term due to the drag of the subphase and a frequency dependent term due to the viscoelastic monolayer.

4.4. Dealing with heterogeneities on the monolayer

In 3D it has been demonstrated[34,59] that the discrepancies found between the rheological behaviour of some systems, when measured with macro- and micro-probes arise from sample heterogeneities at the scale of the microprobe size (a situation encountered rather frequently specially for biological systems). Those discrepancies disappeared when a so-called "two-point" correlation method was used. In this method the displacement of pairs of probe particles (i and j) is cross-correlated for each specific interparticle distance, R_{ij}. Hence, the fluctuations of pairs of particles were measured for all the possible values of R_{ij} within the system. Vector displacements of individual particles were calculated as a function of the lag time, t, for all the initial absolute times, t_0, and the ensemble averaged tensor product of the vector displacements was calculated:[59]

$$D_{\alpha\beta}(r,t) = \langle \Delta r_\alpha^i(r,t) \Delta r_\beta^j(r,t) \delta[r - R_{ij}(t_0)] \rangle_{i \neq j, t_0}$$
$$\Delta r_{\alpha,\beta}^{i,j}(r,t) = r_{\alpha,\beta}^{i,j}(t_0 + t) - r_{\alpha,\beta}^{i,j}(t_0) \tag{13}$$

where α and β are coordinate axes. Usually the experimental coordinates x and y are transformed to parallel (D_{rr}) and perpendicular ($D_{\theta\theta}$) ones. When hydrodynamic interactions between the two particles can be neglected, the average D_{rr} corresponding to $i = j$ represents the one-particle mean square displacement. Two-point microrheology probes the dynamics at different particle separation lengths, from distances much larger than the particle radius down to the particle size, which is equivalent to the extrapolation of long-wavelength thermal fluctuations of the medium to the particle size. This method has been also recently applied to quasi-2D systems,[60,61] in ref. 60 a protein (HSA) adsorbed at the surface of water is studied using 0.9 µm carboxyl-modified PS particles, and they found that the layer is essentially viscous, $D_{rr} \approx t$, and that D_{rr} scales as $1/r$ (like in a 3D system) for low surface viscosities and almost as $\ln r$ for high surface viscosities; in a true 2D system a $\sim\log r$ dependence of D_{rr} is expected.

5. Results and discussion

As we have said in the Introduction, we have measured the surface shear viscosity of monolayers of PtBA with several molecular weights ranging from a thousand to a million Dalton, however here we will show in detail only results of two of them: one below and the other above a critical size of 12.8 kDa (about 100 monomers).[22] Above this limit the Flory radius scales as $R_F \approx N^{3/4}$ whereas below that limit it scales as $R_F \approx N$.[62,63] The results found for the polymers in the whole M_w range studied are qualitatively equal to those of these two polymers taken as typical examples.

5.1. Mean square displacements and diffusion coefficients

5.1.1. The bare air–water interface. In order to obtain the shear surface viscosity of monolayers by particle tracking it is necessary to discuss first the diffusion coefficients of the particles probes moving on a polymer-free interface, D_0. One important point that should be considered is that the motion of particles trapped at a fluid interface is strongly influenced by particle–particle interactions, specially for charged particles that are known to interact by a long-range dipolar repulsive interaction.[52] As already discussed in the Techniques and Data Analysis section all the measurements have been performed with a low particle surface coverage fraction ($\phi < 0.01$) where the experimental diffusion coefficient is essentially the infinite dilution one, D_0. The experimental values for all the particles (Table 2) agree with Fischer's calculations for $B = 0$ using experimental contact angles and a scaling factor $\mathscr{R} = 1.8 \pm 0.2$ (eqn (8)).

5.1.2. MSD of particles in PtBA monolayers. Both the absolute and the relative mean squared displacement, $\langle \Delta r^2(t) \rangle$, measured were linear at short lag times indicating a pure diffusive motion [$\alpha = 1$ in eqn (1) and (2)], while it is sub-diffusive ($\alpha < 1$) for longer lag times, depending on both surface concentration and molecular weight. In what follows only the linear part of $\langle \Delta r^2(t) \rangle$ vs. t will be discussed for calculating the surface viscosity

using Fischer's theory, while the whole time interval will be used when the GSE approach is used.

Let us first discuss the results for the polymer with a low molecular weight. Fig. 1 shows the MSD of PMMA particles with a diameter of 2 μm in a PtBA (M_w = 4.6 kDa) monolayer as a function of time and for different surface concentrations. As expected the monotonic decrease in the MSD with increasing Γ reflects an increase in the surface shear viscosity of the monolayer.

Fig. 2 shows the short time diffusion coefficient, D, of the different particles used as probes as a function of Γ. The comparison of the results for SiO$_2$ particles (σ = 1 μm), PMMA (σ = 1 μm and 2 μm), as well as for PS particles (σ = 1.6 μm), indicates that the surface chemical nature of the particles has only a very slight effect on D in spite of the noticeable differences in θ. As expected, increasing σ reduces D in a Stokes-like fashion and in all the cases D decreases as Γ increases.

5.2. Shear viscosities using Fischer's theory

In order to calculate the surface shear viscosity η_s of PtBA monolayers as a function of Γ from the short time diffusion coefficients we have used the numerical method proposed by Fischer et al.[50] (eqn (5)–(8)). The experimental θ values at a bare air/water interface with surface tension, γ_w, for each type of particle, were corrected by using the Young's equation that accounts for the θ dependence on the surface tension, $\gamma = \gamma_w - \Pi$, at increasing polymer concentration. It must be stressed that for the values of θ shown in Table 2 the θ-dependences of the coefficients k_T^i are much weaker than for more hydrophobic particles.[50]

Fig. 2 Short time diffusion coefficient, D, of different microparticles as a function of the surface concentration Γ of a PtBA monolayer (4.6 kDa): (a) PMMA particles with σ = 1 μm (▲) and 2 μm (▽). (b) PS particles (σ = 1.6 μm) (■) and SiO$_2$ (σ = 1 μm) (◇). (c) PS particles (σ = 5.7 μm) (●). (d) Diffusion coefficient D relative to the diffusion coefficient of the bare water surface, D_0; symbols as in (a), (b), and (c).

The dependence of η_s on the surface concentration of PtBA monolayer with M_w = 4.6 kDa and 103 kDa is shown in Fig. 3. We have included the entire experimental set of shear viscosities obtained from the measurements of D using different particles as tracers. The observed surface shear viscosity values range from 1×10^{-10} to 1.25×10^{-9} N s m^{-1} for the lower molecular weight, and 1×10^{-10} to 4.5×10^{-8} for the higher one. Particles with different chemical natures and sizes lead to almost identical shear viscosity values in the whole Γ-range studied. This agreement of the η_s data measured with different probe particles indicates that the particle type or its surface nature does not affect the η_s measurements and that Fischer's calculations correctly account
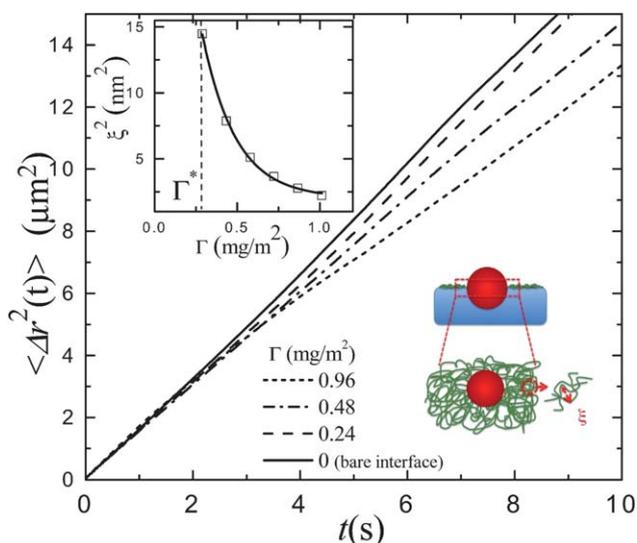

Fig. 1 Time evolution of the mean square displacement of PMMA particles (σ = 2 μm) for different surface concentrations of a PtBA monolayer (M_w = 4.6 kDa). Upper inset: square of the mesh size ξ as a function of Γ. Note that the MSD of the particles are much larger than ξ^2. Vertical straight line marks the overlapping concentration Γ^*. Lower inset: sketch of the quasi-2D system formed by the polymer with $\xi \approx$ O (nm) and a particle with $\sigma \approx$ O(μm).
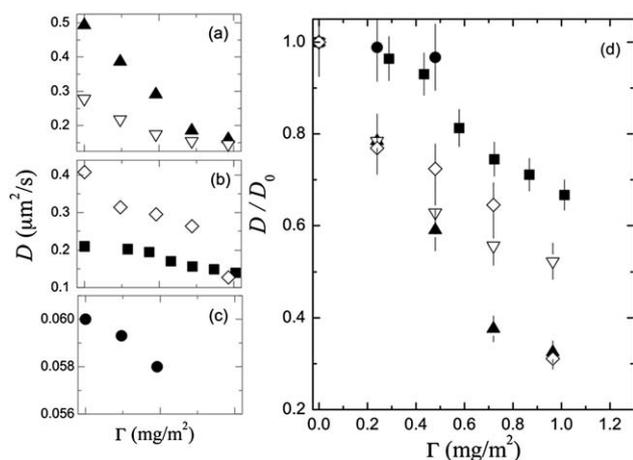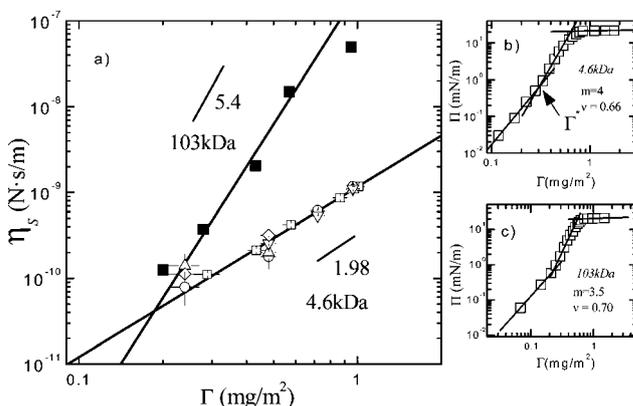

Fig. 3 (a) Surface shear viscosity, η_s, as a function of the surface concentration, Γ, of PtBA monolayers (4.6 kDa and 103 kDa). Symbols correspond to different particles used as tracers: (■, □) PS (σ = 1.6 μm); (◇) PS (σ = 5.7 μm); (○) PMMA (σ = 2 μm); (△) PMMA (σ = 1 μm); (▽) SiO$_2$ (σ = 1 μm). The straight lines correspond to a power law dependence, $\eta_s \sim \Gamma^\beta$. Π–Γ Isotherm of the PtBA monolayers (b) 4.6 kDa and (c) 103 kDa. Γ^* marks the start of the semidilute regime where the power law description is plausible obtaining Flory exponents of ν = 0.66 ± 0.02 and 0.7 ± 0.03.

for the size and θ-dependence of the friction coefficients. A similar result can be reached using Danov's theory.[51] (results not shown) thus pointing out that for the present monolayers the assumption of incompressible (Fischer's theory) or compressible (Danov's theory) character does not play a significant role. This is in agreement with the conclusions of Sickert *et al.*[43] for fatty acid monolayers. The lack of a specific particle surface effect on the shear viscosity of PtBA monolayers suggests that there is not a significant effect of the polymer–particle interactions on the shear viscosity of these monolayers. We have fitted the experimental data to the following power-law dependency $\eta_s \approx \Gamma^\beta$, the continuous line in Fig. 3 shows the fit with $\beta = 1.98 \pm 0.06$ for 4.6 kDa and $\beta = 5.4 \pm 0.2$ for 103 kDa.

Taking into account the theoretical argument proposed by de Gennes[6,64] for the PtBA monolayer with the lower molecular weight (4.6 kDa), corresponding to a chain size $N = 46$, smaller than the critical one ($N_e \approx 100$),[65] it is possible to describe the surface shear viscosity by the Rouse-like dynamics:

$$\eta_{Rouse} = Nl\left(l^2\Gamma\right)^{\nu-1/1-2\nu} \tag{14}$$

where l is the monomer length and ν is the Flory exponent for the radius of gyration ($R_F \approx N^\nu$). This model assumes that the force exerted on a polymeric coil is the hydrodynamic drag force exerted by the subphase. Hence, the surface shear viscosity has its origin in the hydrodynamic coupling of the coils to the subphase. If we relate the experimental scaling exponent β with the scaling description of η_s provided by the Rouse model, one can write the relation $\nu = (\beta + 1)/(1 + 2\beta)$ which leads to a value that corresponds to $\nu = 0.60 \pm 0.05$. This demonstrates that the PtBA coils (for $N < N_e$) in a quasi-2D scenario are strongly segregated, and entanglements may appear only in the soft periphery of the coil thus playing a minor role. From the Π–Γ isotherm (Fig. 3b) we have obtained a Flory exponent[6,64] of $\nu = 0.66 \pm 0.02$ which is compatible with the one obtained from the shear viscosity measurements by means of the Rouse model proposed for these experimental conditions. These results point out the absence of entanglement as expected for polymer monolayers below N_e.

Let us now discuss the results obtained for monolayers formed with the higher molecular weight ($N > N_e$) PtBA for which it has been demonstrated that chain entanglements exist above Γ^*.[22] In this case, using PS particles ($\sigma = 1.6$ μm) as tracers, we found $\beta = 5.4 \pm 0.2$. The different values of β (from 1.98 to 5.4) for the two molecular weights could be due not only to the existence of inter-chain frictions at the periphery of the polymer coils, but also to internal frictions as expected for flexible PtBA chains, long enough to entangle in the monolayer, thus leading to an additional energy dissipation. The behaviour found for PtBA with 103 kDa is close to the one expected for an entangled network where the viscous friction scales with an exponent β close to 6.[6] The Flory exponent obtained from the scaling analysis of the Π–Γ isotherm (Fig. 3c), is 0.70 ± 0.03 compatible with the description of a system in terms of a *good-solvent* scenario where the entanglements may exist.[64]

5.3. Comparison between micro and macro-rheology

5.3.1. Dependence of surface shear viscosity on surface concentration. The values of η_s obtained from particle tracking are more than three orders of magnitude lower than the values

measured by conventional macroscopic rheometers as it can be seen in Fig. 4. However, the power-law found for the shear viscosity, $\eta_s\Gamma^\beta$ is similar for macro- ($\beta = 6$) and micro-rheology ($\beta = 5.4$). The discrepancy between the values of η_s obtained from micro- and macro-rheology measurements has no clear answer so far. There might be two possible reasons: (a) *the assumptions of the models* used to derive the surface shear viscosity from the diffusion coefficients; (b) *the existence of heterogeneities in the polymer monolayer* that might arise from a depletion layer created around the particles, thus leading to an effective polymer surface density lower than the average Γ. In the following we will deal with these two possibilities.

5.3.2. Molecular weight effect on the shear viscoelasticity of PtBA monolayer. As pointed out above there is a quantitative inconsistency between macro- and micro-rheology results. Fig. 5 shows clearly this difference for PtBA of different molecular weights at the same experimental conditions. We have measured the surface shear viscosity (η_s) at the so-called Γ^{**} surface concentration ($\Pi^{**} = 16$ mN m^{-1}) for different molecular weights (see Table 1). The shear viscosities obtained from particle tracking which are shown in Fig. 5 have been calculated by using Fischer's calculations (these results coincide, within the combined uncertainties, with those obtained using Danov's theory and the Generalized Stokes Einstein equation, GSE).

From the macroscopic measurements of $\eta_s(\Gamma^{**})$ we have already demonstrated[20] that above the critical size ($N_e \approx 100$), there is a reptation-like dependence of the shear viscosity with the molecular weight ($\eta_s \approx N^{3.0\pm0.3}$) while a weaker linear dependence ($\sim N$) was found below N_e. These values of η_s are in the range of 8×10^{-7} to 3 N s m^{-1}. However, from microrheology measurements we have obtained much lower values of $\eta_s(\Gamma^*)$, for all the samples studied, in the range of 2×10^{-10} to 4×10^{-8} N s m^{-1}. It is interesting to notice that for $N > N_e$ the surface shear viscosities obtained from particle tracking shows the same dependence on the molecular weight ($\eta_s \approx N^{0.9\pm0.2}$) despite the difference in the absolute values with the ones obtained from macrorheology. For $N < N_e$ the particle tracking results give η_s values which are
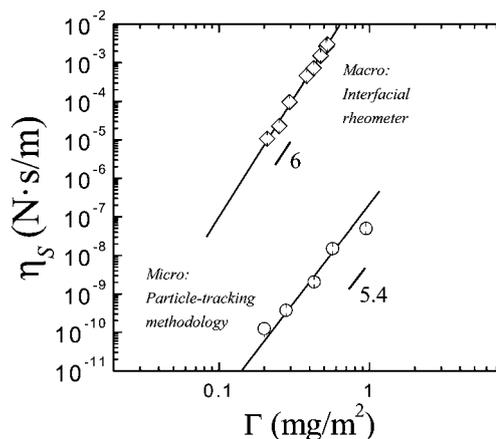
Fig. 4 Surface shear viscosity for a PtBA monolayer with $M_w = 103$ KDa as a function of the surface concentration Γ. ($\bigcirc$) correspond to data obtained from particle-tracking plus Fischer's calculations, whereas ($\diamondsuit$) correspond to data obtained from conventional interfacial shear rheometry.
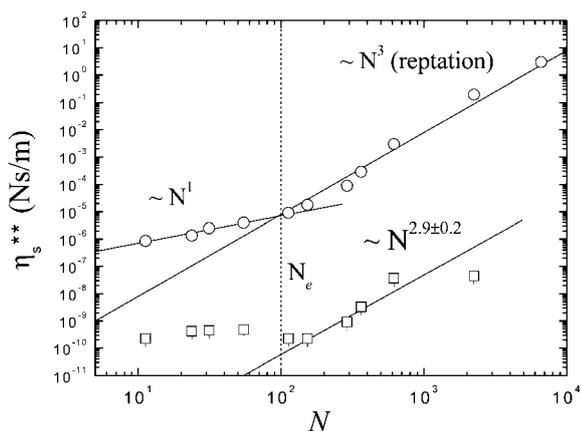
Fig. 5 Surface shear viscosity for monolayers of PtBA as a function of the chain length at a dense state Γ^{**} ($\Pi^{**} = 16$ mN m^{-1}). Open squares correspond to data obtained using particle tracking while the open circles were obtained from conventional oscillatory rheometers. Solid lines in both sets of data represent the scaling behaviour of the shear viscosity with the molecular weight. N_e marks the critical chain length when entanglements between the polymer chains begin.

Fig. 6 Frequency dependence of the storage (G') and loss (G'') moduli of PtBA monolayers (a) $M_w = 4.6$ kDa and $\Gamma = 1.01$ mg m^{-2} and (b) $M_w = 4.6$ kDa, $\Gamma = 0.43$ mg m^{-2} and $M_w = 103$ kDa, $\Gamma = 0.46$ mg m^{-2} obtained from the mean square displacements of PS ($\sigma = 1.6$ μm) and PMMA ($\sigma = 2$ μm) particles using the Generalized Stokes–Einstein equation and the radius of the particles as characteristic length (eqn (12)). Symbols as follows: G' ($\square,\blacksquare$) and G'' ($\bigcirc,\bullet$); straight lines show the power law behaviour of the experimental loss modulus: $G'' \approx \omega^{0.9}$.

almost constant and close to the resolution limit of the technique, in which the drag on the probe particle is dominated by the bulk water phase. These differences cannot be attributed to specific interactions between the particles and the monolayer as it was indicated above. In fact, the results obtained for particles with different surface Chemistry are identical so depletion effects may be discarded, as it was already discussed by Lee *et al.*[41] The agreement of the values of η_s calculated by Fischer's[50] and Danov's[51] methods indicates that the differences found are not due to the different assumptions made by both theories about the hydrodynamic drag of a particle trapped at a viscous interface. One of the problems of these hydrodynamic theories is that they are made for purely viscous interfaces and polymer monolayers above Γ^* are expected to be viscoelastic. Additionally, Fischer's theory has been used to calculate surface viscosity from the short time diffusion coefficients where the MSD is linear with the lag time, neglecting any frequency dependence, *i.e.* assuming a Newtonian behavior for the shear surface viscosity.

5.4. Shear viscoelasticity moduli of PtBA monolayers by using the generalized Stokes–Einstein equation (GSE)

Using the full lag time dependence of the MSD we have calculated the frequency dependence of the surface shear storage (G') and loss (G'') moduli of the PtBA monolayers using Mason's treatment (eqn (12) and (11)), and taking the radius of the particle as the characteristic length to transform the "*apparent*" 3D moduli to the surface ones. Fig. 6 shows G' and G'' for a low 4.6 kDa and a high 103 kDa molecular weight PtBA monolayers calculated from the MSD of PS particles ($\sigma = 1.6$ μm). The accessible frequency range depends on the particle size used as probe, and has been estimated according to Levine and Lubensky.[34] For the lower molecular weight PtBA two surface concentrations are shown in Fig. 6, (a) 1.01 mg m^{-2} and (b) 0.43 mg m^{-2} and for the higher molecular weight (b) 0.46 mg m^{-2}; all above the overlapping concentration, Γ^*. A predominantly
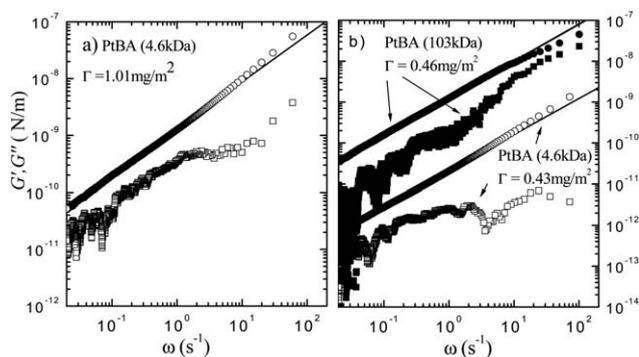
viscous response $G''(\omega) > G'(\omega)$ was observed over the whole surface concentration range and for all the molecular weights. At first sight it may seem surprising that shear viscoelastic response of an entangled monolayer is dominated by the loss term at the frequencies of the experiment. However, the fact that $G'' > G'$ for polymer monolayers when the interface is a good solvent seems to be quite general in the semidilute regime. In fact, E. Spigone *et al.*[16] report, using two different macro-rheometers, that monolayers of PVAc at the air/water interface ("good solvent conditions") have a shear response which is dominated by G'' in the semidiluted regime, with $G'' \approx \omega$. For very dense layers, beyond Γ^{**}, they report a transition characterized by $G'' \approx \omega^{0.5}$ with viscous and elastic modulus with similar magnitude, and they argue that in this very dense state there is a transition in the polymer monolayer from fluid to a soft solid state. Moreover, the macroscopic rheology results for PtBA monolayers give $G'' > G'$ being the values of the storage modulus below the resolution limit of the rheometers except for the highest molecular weights.[22]

In Fig. 6 the loss modulus follows a power law $G'' \approx \omega^{0.9\pm0.1}$, that leads to a weak surface viscosity dependence $\eta_s \approx \omega^{-0.1\pm0.02}$, a similar result has been found for the rest of the molecular weights and surface concentrations. The results obtained with the other particles agree with those shown in Fig. 6.

Fig. 7 shows the values of η_s ($\omega \to 0$) from GSE as a function of the polymer concentration. GSE and Fischers' hydrodynamic calculations lead to similar surface shear viscosities for both PtBA monolayers (when N is smaller or larger than N_e). Furthermore, this is true for probe particles of rather different chemical natures and sizes.

In conclusion, it seems that the models underlying the calculation of the shear viscosities are not the cause of the discrepancy between macro- and micro-rheology results. The agreement between η_s ($\omega \to 0$) obtained from GSE and η_s obtained using the hydrodynamic treatments, for different monolayers and with several types of probe particles, indicates that the inconsistency between macro- and micro-surface rheology is not due to a frequency dependence of the surface viscosity or inconsistency
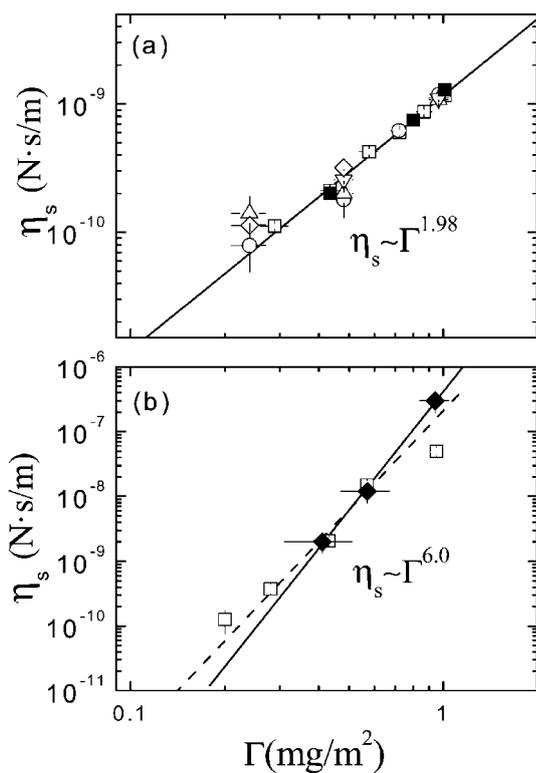
Fig. 7 (a) Surface shear viscosity, η_s, as a function of the surface concentration, Γ, for a PTBA monolayer (4.6 kDa). The η_s values has been calculated from the GSE equation in the limit of low frequency (■: PS particles with diameter 1.6 μm). We also include the η_s values obtained using Fischer's calculations (open symbols). Symbols correspond to different particles used as tracers: (□) PS ($\sigma = 1.6$ μm); (◇) PS ($\sigma = 5.7$ μm); (○) PMMA ($\sigma = 2$ μm); (△) PMMA ($\sigma = 1$ μm); (▽) SiO₂ ($\sigma = 1$ μm). The continuous line shows the power law dependency $\eta_s \sim \Gamma^{1.98\pm0.06}$. (b) Γ-dependence of η_s for a PTBA monolayer with higher molecular weight (103 kDa). Filled symbol ◆ corresponds to the GSE method using PMMA particles (2 μm), and open ones correspond for Fischer's method using PS particles (1.6 μm). The continuous line shows the power law dependency $\eta_s \sim \Gamma^{6\pm0.2}$ obtained with the GSE calculation. Dashed line shows the power law $\eta_s \sim \Gamma^{5.4 \pm 0.3}$ describing the values obtained with Fischer's method.

of the hydrodynamic model that treat the surface as purely viscous. We must recall that the η_s values found by the GSE approach contain both the subphase viscosity (frequency independent) and the monolayer viscosity (frequency dependent). In spite of this, the shear viscosities found by GSE and Fischer's treatment essentially coincide, indicating that the probe drag is basically controlled by the viscoelastic monolayer even for moderated Boussinesq numbers (lower molecular weights). There is an additional point that deserves to be commented, as already said in order to compare the surface viscosities obtained by GSE, Fischer's treatment and macroscopic rheometry, the viscoelastic moduli have been transformed to 2D units using the radius of the particle, in this sense we use the same approach as the macroscopic rheometers that use experimental constants related to the characteristic size of the probes that generates the flow, to get the surface moduli.

In what follows the possibility of effects arising from spatial heterogeneities in the monolayers will be discussed.

5.5. Two-particle microrheology of PtBA monolayers

As it was mentioned in the Data Analysis section, two-point microrheology is based on cross correlating the motion of pairs of particles. We follow the thermal motion of several particles using video particle tracking as explained before but now we compute the outer product of two different tracers' vector displacements separated a given distance r at the initial time t_0. Then an ensemble averaging over all trajectory pairs yields a correlation tensor $D_{\alpha\beta}$ (where D_{rr} is the component directed along the line connecting the centres of the two particles for a given distance r) that provides the degree of correlation between particle random motion in the lag time, t, and at a separation distance r. Now the two-point mean-square displacement, $\langle \Delta r^2(t) \rangle_D$, is defined as,[57]

$$\langle \Delta r^2(t) \rangle_D = \frac{2r}{a} D_{rr}(r, t) \qquad (15)$$

This expression accounts for the thermal motion obtained by the extrapolation of the long-wavelength thermal fluctuations of the medium down to the bead size, a. In practice, we have obtained the respective D_{rr} over the length scale from 3.2 to 80 μm, and then we have extrapolated D_{rr} to the probe size to calculate $\langle \Delta r^2(t) \rangle_D$.

Fig. 8 shows the short time average $\langle D_{rr}(r,t)/t \rangle$ as a function of r for two PtBA monolayers: (a) molecular weight 4.6 kDa at a surface concentration of $\Gamma = 1.01$ mg m⁻² and (b) molecular weight 103 kDa at a surface concentration of $\Gamma = 0.43$ mg m⁻². These measurements correspond to the particle-tracking experiments performed with PS particles ($\sigma = 1.6$ μm) and
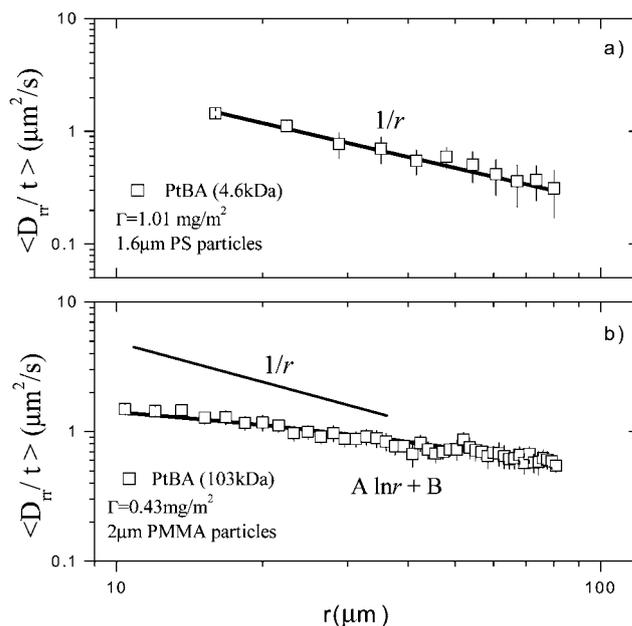

Fig. 8 Lag time average two-point correlation function $\langle D_{rr}(r,t)/t \rangle$ as a function of r. (a) Monolayer of PtBA (4.6 kDa) at a surface concentration of 1.01 mg m⁻² using as probe PS particles ($\sigma = 1.6$ μm) and (b) Monolayer of PtBA (103 kDa) at a surface concentration of 0.43 mg m⁻² using as probe PMMA particles ($\sigma = 2$ μm). It can be observed that the correlation functions have the following dependences $\langle D_{rr}(r,t)/t \rangle \approx 1/r$ for the lower molecular weight and $\langle D_{rr}(r,t)/t \rangle \approx A \ln r + B$, where A and B are constants.

PMMA ($\sigma = 2$ µm), respectively. It is noticeable that $D_{rr} \approx 1/r$ for the lower molecular weight which is the expected result for a 3D system, or as in our case, for a quasi-2D system with a relatively low surface shear viscosity as the monolayer of PtBA 4.6 kDa ($N < N_e$). In these conditions the motion of a tracer particle creates a flow field that affects the motion of other particles and decays as one moves far from the particle mainly by the coupling with the water bulk subphase. Hence, the correlated motions (D_{rr}) decay as a function of particle separation ($\sim 1/r$) for the short lag times considered, $D_{rr} \approx t$. In contrast, for the higher molecular weight monolayers we found a logarithmic dependence on r. A similar result has been found by Prasad and Weeks[61] for soap films of varying thickness, when the film thickness approaches the particle size, and by Prasad et al.[60] for HSA monolayers with high surface viscosity and indicates a transition from a hydrodynamic behaviour influenced by the water subphase (3D like) to a 2D dominated one at high surface viscosities. We must recall that for the PtBA monolayers, independent of the molecular weight, the ellipsometric thickness ranges from 1 to 7 nm,[22] much smaller than the probe particle sizes.

Fig. 9a shows the time dependence of $\langle \Delta r^2(t) \rangle$ and $\langle \Delta r^2(t) \rangle_D$ for the same PtBA monolayers considered in Fig. 8a. Single and two-point mean square displacements coincide, which point out that local heterogeneities, if there are any, do not affect the measurements of the MSD's. In contrast, Fig. 9b corresponding
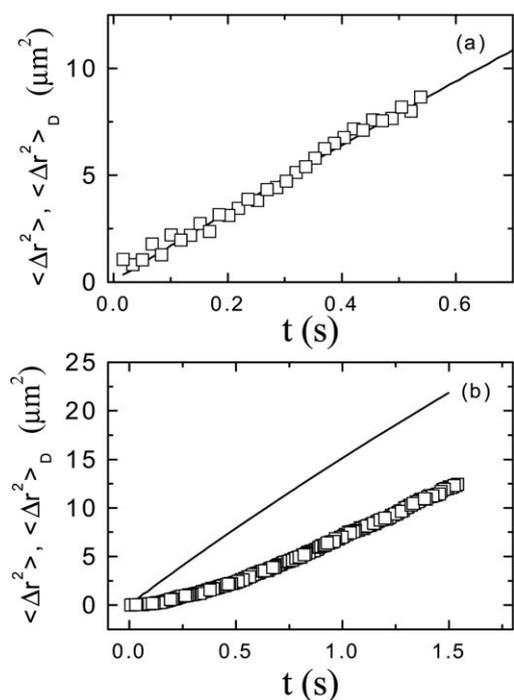

Fig. 9 (a) Time dependence of the two-point mean-square displacement $\langle \Delta r^2(t) \rangle_D$ (□) and single particle mean square displacement $\langle \Delta r^2(t) \rangle$ (straight line) for PS beads with diameter 1.6 mm attached at a air–water interface where a PtBA monolayer (4.6 kDa, $\Gamma = 1.01$ mg m^{-2}) has been previously spread. (b) The same as in (a) for a PtBA monolayer, 103 kDa molecular weight and $\Gamma = 0.43$ mg m^{-2} using 2 µm diameter PMMA particles.

to the higher molecular weight (103 kDa) ($N > N_e$) PtBA monolayer, shows that $\langle \Delta r^2(t) \rangle$ is larger than $\langle \Delta r^2(t) \rangle_D$, suggesting that the motion of the beads may be affected by the presence of heterogeneities in the monolayer.

Although, there may be some degree of heterogeneity in the higher molecular weight PtBA monolayers, this does not seem to be a key factor in order to explain the gap between macro- and micro-surface shear viscosity measurements. In fact if one takes the surface shear viscosity data obtained with macro-rheometers for the higher molecular weights monolayers and plug these values into eqn (8) to calculate the diffusion coefficients of the probe motion, the result would be $\sim 10^{-7}$–10^{-8} µm^2 s^{-1} in other words the probe particle would be tied to their initial position and would not move during the experimental time.

One additional question that deserves a further comment is the comparison between the strain exerted in macro- and micro-rheometers. In passive particle tracking, the kind of experiments presented here, the strain amplitude arises essentially from the thermal energy and so it takes the lowest possible value in contrast to the strains imposed by the probes of the two macrorheometers used that are higher. However, as already mentioned, all the measurements performed with the macro-rheometers were done well inside the linear response regime.

Conclusions

We have demonstrated the validity of the video particle tracking approach for measuring the surface rheology of polymer Langmuir monolayers at the air–water interface.

We have also demonstrated that neither the different chemical natures and sizes of particle probes nor the model used to derive the viscosity from MSD (Fischer's model or GSE) affect the obtained results, making particle tracking microrheology self-consistent.

We have focused here on the viscoelastic response of the PtBA monolayers in different experimental conditions. We have found that microrheological experiments lead to values of the shear viscosity up to three orders of magnitude lower than the ones measured by conventional macroscopic rheometers. We have discarded several possible causes of the quantitative discrepancy, some of them already mentioned in, ref. 41 by combining measurements using particles of different sizes and surface chemistry, and by comparing the predictions of different theoretical approaches that lead to very similar values of the surface shear viscosity. Therefore it is clear that the discrepancy is not due to model limitations, frequency dependence effects or heterogeneity of the monolayer at the scale of the probe size. In any case, as pointed out for 3D systems in ref. 66 and 67 it must be taken into account that micro- and macro-surface shear viscosities might not have the same physical meaning. Experiments done with a magnetic needle rheometer with several needle sizes (and therefore different values of the Boussinesq number) on the same monolayer might shed light on this problem.[25]

In spite of the differences found between macro- and micro-rheology absolute surface shear viscosity results, we show that both macro- and micro-experimental data follow the same scaling laws. Our results suggest that long enough flexible PtBA chains can entangle in the monolayer showing a reptation-like motion.

Acknowledgements

References

1   R. A. L. Jones and R. W. Richards, *Polymers at Surfaces and Interfaces*, Cambridge Univ. Press, Cambridge, 1999.
2   *Langmuir-Blodgett Films*, ed. G. Roberts, Plenum, New York, 1990.
3   D. Langevin, *Adv. Colloid Interface Sci.*, 2000, **88**, 209–222.
4   J. Maldonado-Valderrama, A. Martín-Molina, A. Martín-Rodríguez, M. A. Cabrerizo-Vilchez, M. J. Galvez-Ruiz and D. Langevin, *J. Phys. Chem. C*, 2007, **111**, 2715–2723.
5   L. H. Sperling, *Polymeric Multicomponent Materials*, Wiley Interscience, New York, 1997.
6   P.-G. de Gennes, *Scaling Concepts in Polymer Physics*, Cornell University Press, Ithaca, 1979.
7   A. R. Esker, C. Kim and H. Yu, *Functional Materials and Biomaterials*, 2007, vol. 209, pp. 59–110.
8   R. Vilanove and F. Rondelez, *Phys. Rev. Lett.*, 1980, **45**, 1502.
9   F. Monroy, H. M. Hilles, F. Ortega and R. G. Rubio, *Phys. Rev. Lett.*, 2003, **91**.
10 P. Cicuta, E. J. Stancik and G. G. Fuller, *Phys. Rev. Lett.*, 2003, **90**, 236101/1–236101/4.
11 F. Monroy, F. Ortega, R. G. Rubio and M. G. Velarde, *Adv. Colloid Interface Sci.*, 2007, **134–35**, 175–189.
12 C. F. Brooks, G. G. Fuller, C. W. Frank and C. R. Robertson, *Langmuir*, 1999, **15**, 2450–2459.
13 A. R. Esker, C. Kim and H. Yu, *Adv. Polym. Sci.*, 2007, **209**, 59.
14 S. Rivillon, F. Monroy, F. Ortega and R. G. Rubio, *Eur. Phys. J. E: Soft Matter Biol. Phys.*, 2002, **9**, 375–385.
15 C. Luap and W. A. Goedel, *Macromolecules*, 2001, **34**, 1343–1351.
16 E. Spingone, G.-Y. Cho, G. G. Fuller and P. Cicuta, *Langmuir*, 2009, **25**, 7457–7464.
17 S. A. Sukhishvili, Y. Chen, J. D. Muller, E. Gratton, K. S. Schweizer and S. Granick, *Macromolecules*, 2002, **35**, 1776–1784.
18 G. T. Gavranovic, J. M. Deutsch and G. G. Fuller, *Macromolecules*, 2005, **38**, 6672–6679.
19 J. Kumaki, T. Kawauchi and E. Yashima, *J. Am. Chem. Soc.*, 2005, **127**, 5788–5789.
20 X. Wang and V. J. Foltz, *J. Chem. Phys.*, 2004, **121**, 8158–8162.
21 J. Kumaki, T. Kawauchi and E. Yashima, *Macromolecules*, 2006, **39**, 1209–1215.
22 A. Maestro, H. Hilles, F. Ortega, R. G. Rubio, D. Langevin and F. Monroy, *Soft Matter*, 2010, **6**, 4407–4412.
23 J. Krägel, S. Siegel, R. Miller, M. Born and K.-H. Schano, *Colloids Surf., A*, 1994, **91**, 169–180.
24 P. Erni, P. Fischer, E. J. Windhab, V. Kusnezov, H. Stettin and J. Läuger, *Rev. Sci. Instrum.*, 2003, **74**(11), 4916–4924.
25 S. Reynaert, C. F. Brooks, P. Moldenaers, J. Vermant and G. G. Fuller, *J. Rheol.*, 2008, **52**(1), 261–285.
26 C. Barentin, C. Ybert, J. di Meglio and J. Joanny, *J. Fluid Mech.*, 1999, **397**, 331–349.
27 F. Monroy, F. Ortega and R. G. Rubio, *J. Phys. Chem. B*, 1999, **103**, 2061–2071.
28 J. Wu and L. Dai, *Appl. Phys. Lett.*, 2006, **89**, 094107.
29 T. G. Mason, *Rheol. Acta*, 2000, **39**, 371–378.
30 T. A. Waigh, *Rep. Prog. Phys.*, 2005, **68**, 685–742.
31 P. Cicuta and A. Donald, *Soft Matter*, 2007, **3**, 1449–1495.
32 M. L. Gardel, M. T. Valentine and D. A. Weitz, in *Microscale Diagnostic Techniques*, ed. K. Brauer, Springer, Berlin, 2005.
33 A. Mukhopadhayay and S. Granick, *Curr. Opin. Colloid Interface Sci.*, 2001, **6**, 423–429.
34 A. J. Levine and T. C. Lubensky, *Phys. Rev. Lett.*, 2000, **85**, 1774–1777.
35 T. G. Mason and D. A. Weitz, *Phys. Rev. Lett.*, 1995, **74**, 1250–1253.
36 R. M. Evans, M. Tassieri, D. Auhl and T. A. Waigh, *Phys. Rev. Lett.*, 2009, **80**, 012501.
37 C. Barentin, P. Muller, C. Ybert, J. Joanny and J.-M. di Loglio, *Eur. Phys. J. E: Soft Matter Biol. Phys.*, 2000, **2**, 153–159.
38 H. M. Hilles, H. Ritacco, F. Monroy, F. Ortega and R. G. Rubio, *Langmuir*, 2009, **25**, 11528–11532.
39 S. Reynaert, C. F. Brooks, P. Moldenaers, J. Vermant and G. G. Fuller, *J. Rheol.*, 2008, **52**, 261–285.
40 A. Maestro, F. Ortega, F. Monroy, J. Krägel and R. Miller, *Langmuir*, 2009, **25**, 7393–7400.
41 M. H. Lee, D. H. Reich, K. J. Stebe and R. L. Leheny, *Langmuir*, 2010, **26**, 2650–2658.
42 F. Ortega, H. Ritacco and R. G. Rubio, *Curr. Opin. Colloid Interface Sci.*, 2010, **15**, 237–245.
43 M. Sickert, F. Rondelez and H. A. Stone, *EPL*, 2007, **79**, 66005.
44 L. J. Bonales, H. Ritacco, J. E. F. Rubio, R. G. Rubio, F. Monroy and F. Ortega, *Open Phys. Chem. J.*, 2007, **1**, 25–32.
45 A. Maestro, L. J. Bonales, H. Ritacco, R. G. Rubio and F. Ortega, *Phys. Chem. Chem. Phys.*, 2010, **12**, 14115–14120.
46 V. N. Paunov, *Langmuir*, 2003, **19**, 7970–7976.
47 T. S. Horozov, D. A. Braz, P. D. I. Fletcher, B. P. Binks and J. H. Clint, *Langmuir*, 2008, **24**, 1678–1681.
48 J. H. Clint and S. E. Taylor, *Colloids Surf., A*, 1992, **65**, 61–67.
49 D. O. Grigoriev, J. Krägel, V. Dutschk, R. Miller and H. Möhwald, *Phys. Chem. Chem. Phys.*, 2007, **9**, 6447–6454.
50 T. M. Fischer, P. Dhar and P. Heinig, *J. Fluid Mech.*, 2006, **558**, 451–475.
51 R. Dimova, K. Danov, B. Pouligny and I. B. Ivanov, *J. Colloid Interface Sci.*, 2000, **226**, 35–43.
52 L. J. Bonales, J. E. F. Rubio, H. Ritacco, C. Vega, R. G. Rubio and F. Ortega, *Langmuir*, 2011, **27**, 3391–3400.
53 J. F. Klinger and H. M. McConnell, *J. Chem. Phys.*, 1993, **97**, 6096–6100.
54 J. Krägel and S. Derkatch, in *Interfacial Rheology*, ed. R. Miller and L. Liggieri, Brill, Leiden, 2009.
55 A. Maestro, F. Ortega, F. Monroy, J. Krägel and R. Miller, *Langmuir*, 2009, **25**, 7393–7400.
56 A. M. Corrigan and A. Donald, *Soft Matter*, 2010, **6**, 4105–4111.
57 Y. Gambin, R. Lopez-Esparza, M. Feffay, E. Sierecki, N. S. Gov, M. Genest, R. S. Hodges and W. Urbach, *Proc. Natl. Acad. Sci. U. S. A.*, 2006, **103**, 2098–2102.
58 J. Wu and L. L. Dai, *Langmuir*, 2007, **23**, 4324.
59 J. C. Croker, M. T. Valentine, E. R. Weeks, T. Gisler, P. D. Kaplan, A. G. Yodh and D. A. Weitz, *Phys. Rev. Lett.*, 2000, **85**, 888–891.
60 V. Prasad, S. A. Koehler and E. R. Weeks, *Phys. Rev. Lett.*, 2006, **97**, 176001.
61 V. Prasad and E. R. Weeks, *Phys. Rev. Lett.*, 2009, **102**, 178302.
62 P.-G. de Gennes, *Scaling Concepts in Polymer Physics*, Cornell University Press, Ithaca, 1979.
63 M. Doi and S. F. Edwards, *The Theory of Polymer Dynamics*, Oxford, Clarendon, 1986.
64 P.-G. de Gennes, Motion of Polymer Near a Solid Surface, in *Liquids at interfaces*, ed. J. Charvolin, J. F. Joanny and J. Zinn-Justin, Elsevier publishers, Les Houches, 1988, Session XLVIII, p. 311.
65 F. Monroy, F. Ortega, R. G. Rubio and B. Noskov, in *Interfacial Rheology*, ed. R. Miller and L. Liggieri, Brill, Leiden, 2009.
66 T. M. Squires and T. G. Mason, *Annu. Rev. Fluid Mech.*, 2010, **42**, 413–438.
67 A. S. Khair and J. F. Brady, *J. Rheol.*, 2008, **52**(1), 165–196.